UNIVERSITY OF BATH

University of Bath

Nonlinear optics in the LP$_{02}$ higher-order mode of a fiber

Y. Chen,[1] Z. Chen,[1,2] W. J. Wadsworth,[1] and T. A. Birks[1,*]

[1]*Department of Physics, University of Bath, Claverton Down, Bath BA2 7AY, UK*
[2]*Visiting from College of Optoelectronics Science and Engineering, National University of Defense Technology, Changsha, 410073, China*
[*]*t.a.birks@bath.ac.uk*

Abstract: The distinct disperion properties of higher-order modes in optical fibers permit the nonlinear generation of radiation deeper into the ultraviolet than is possible with the fundamental mode. This is exploited using adiabatic, broadband mode convertors to couple light efficiently from an input fundamental mode and also to return the generated light to an output fundamental mode over a broad spectral range. For example, we generate visible and UV supercontinuum light in the LP$_{02}$ mode of a photonic crystal fiber from sub-ns pulses with a wavelength of 532 nm.

OCIS codes: (060.5295) Photonic crystals; (060.4370) Nonlinear optics.

References and links

1. J. K. Ranka, R. S. Windeler, and A. J. Stentz, "Visible continuum generation in air-silica microstructure optical fibers with anomalous dispersion at 800 nm," Opt. Lett. **25**(1), 25–27 (2000).
2. J. E. Sharping, M. Fiorentino, A. Coker, P. Kumar, and R. S. Windeler, "Four-wave mixing in microstructure fiber," Opt. Lett. **26**(14), 1048–1050 (2001).
3. W. J. Wadsworth, N. Y. Joly, J. C. Knight, T. A. Birks, F. Biancalana, and P. St. J. Russell, "Supercontinuum and four-wave mixing with Q-switched pulses in endlessly single-mode photonic crystal fibres," Opt. Express **12**(2), 299–309 (2004).
4. J. C. Travers, S. V. Popov, and J. R. Taylor, "Extended blue supercontinuum generation in cascaded holey fibers," Opt. Lett. **30**(23), 3132–3134 (2005).
5. J. H. V. Price, T. M. Monro, H. Ebendorff-Heidepriem, F. Poletti, P. Horak, V. Finazzi, J. Y. Y. Leong, P. Petropoulos, J. C. Flanagan, G. Brambilla, X. Feng, and D. J. Richardson, "Mid-IR supercontinuum generation from nonsilica microstructured optical fibers," IEEE J. Sel. Top. Quantum Electron. **13**(3), 738–749 (2007).
6. J. M. Dudley, G. Genty, and S. Coen, "Supercontinuum Generation in Photonic Crystal Fiber," Rev. Mod. Phys. **78**(4), 1135–1184 (2006).
7. J. M. Dudley and J. R. Taylor, eds., Supercontinuum Generation in Optical Fibers (Cambridge Univ. Press, Cambridge, 2010).
8. J. M. Stone and J. C. Knight, "From zero dispersion to group index matching: how tapering fibers offers the best of both worlds for visible supercontinuum generation," Opt. Technol. **18**(5), 315–321 (2012).
9. J. van Howe, J. H. Lee, S. Zhou, F. Wise, C. Xu, S. Ramachandran, S. Ghalmi, and M. F. Yan, "Demonstration of soliton self-frequency shift below 1300 nm in higher-order mode, solid silica-based fiber," Opt. Lett. **32**(4), 340–342 (2007).
10. S. Ramachandran, Z. Wang, and M. Yan, "Bandwidth control of long-period grating-based mode converters in few-mode fibers," Opt. Lett. **27**(9), 698–700 (2002).
11. G. Stepniak, L. Maksymiuk, and J. Siuzdak, "Binary-phase spatial light filters for mode-selective excitation of multimode fibers," J. Lightwave Technol. **29**(13), 1980–1987 (2011).
12. J. Carpenter and T. D. Wilkinson, "Characterization of multimode by selective mode excitation," J. Lightwave Technol. **30**(10), 1386–1392 (2012).
13. J. M. Dudley, L. Provino, N. Grossard, H. Maillotte, R. S. Windeler, B. J. Eggleton, and S. Coen, "Supercontinuum generation in air-silica microstructured fibers with nanosecond and femtosecond pulse pumping," J. Opt. Soc. Am. B **19**(4), 765–771 (2002).
14. A. Mussot, T. Sylvestre, L. Provino, and H. Maillotte, "Generation of a broadband single-mode supercontinuum in a conventional dispersion-shifted fiber by use of a subnanosecond microchip laser," Opt. Lett. **28**(19), 1820–1822 (2003).
15. C. Lesvigne, V. Couderc, A. Tonello, P. Leproux, A. Barthélémy, S. Lacroix, F. Druon, P. Blandin, M. Hanna, and P. Georges, "Visible supercontinuum generation controlled by intermodal four-wave mixing in microstructured fiber," Opt. Lett. **32**(15), 2173–2175 (2007).
16. R. Cherif, M. Zghal, L. Tartara, and V. Degiorgio, "Supercontinuum generation by higher-order mode excitation in a photonic crystal fiber," Opt. Express **16**(3), 2147–2152 (2008).

17. P. Nandi, Z. Chen, A. Witkowska, W. J. Wadsworth, T. A. Birks, and J. C. Knight, "Characterization of a photonic crystal fiber mode converter using low coherence interferometry," Opt. Lett. **34**(7), 1123–1125 (2009).
18. K. Lai, S. G. Leon-Saval, A. Witkowska, W. J. Wadsworth, and T. A. Birks, "Wavelength-independent all-fiber mode converters," Opt. Lett. **32**(4), 328–330 (2007).
19. A. V. Gorbach and D. V. Skryabin, "Light trapping in gravity-like potentials and expansion of supercontinuum spectra in photonic-crystal fibers," Nat. Photonics **1**(11), 653–657 (2007).
20. J. M. Stone and J. C. Knight, "Visibly "white" light generation in uniform photonic crystal fiber using a microchip laser," Opt. Express **16**(4), 2670–2675 (2008).
21. G. P. Agrawal, *Nonlinear Fiber Optics*, 4th Ed. (Academic Press, 2007).
22. T. A. Birks, D. Mogilevtsev, J. C. Knight, and P. St. J. Russell, "Dispersion compensation using single material fibers," IEEE Photon. Technol. Lett. **11**, 674–676 (1999).
23. S. G. Leon-Saval, T. A. Birks, W. J. Wadsworth, P. St J Russell, and M. W. Mason, "Supercontinuum generation in submicron fibre waveguides," Opt. Express **12**(13), 2864–2869 (2004).
24. A. W. Snyder and J. D. Love, *Optical Waveguide Theory* (Chapman and Hall, London, 1983) p. 253.
25. G. J. Pearce, T. Hedley, and D. M. Bird, "Adaptive curvilinear coordinates in a plane-wave solution of Maxwell's equations in photonic crystals," Phys. Rev. B **71**(19), 195108 (2005).
26. J. C. Knight, J. Arriaga, T. A. Birks, A. Ortigosa-Blanch, W. J. Wadsworth, and P. St. J. Russell, "Anomalous dispersion in photonic crystal fiber," IEEE Photon. Technol. Lett. **12**(7), 807–809 (2000).
27. M. Delgado-Pinar, P. J. Mosley, J. C. Knight, T. A. Birks, and W. J. Wadsworth, "Visible supercontinuum generation in the femtosecond regime in submicron structures," *Nonlinear Photonics Topical Meeting* (Karlsruhe), paper NWD3 (2010).
28. C. D. Poole, J. M. Wiesenfeld, D. J. DiGiovanni, and A. M. Vengsarkar, "Optical fiber-based dispersion compensation using higher order modes near cutoff," J. Lightwave Technol. **12**(10), 1746–1758 (1994).
29. J. D. Joannopoulos, S. G. Johnson, J. N. Winn, and R. D. Meade, *Photonic Crystals,* 2nd Ed. (Princeton Univ. Press, 2008).
30. I. Gris-Sánchez, B. J. Mangan, and J. C. Knight, "Reducing spectral attenuation in small-core photonic crystal fibers," Opt. Mater. Express **1**(2), 179–184 (2011).
31. L. Skuja, "Optically active oxygen-deficiency-related centers in amorphous silicon dioxide," J. Non-Cryst. Solids **239**(1-3), 16–48 (1998).
32. K. Kajihara, L. Skuja, M. Hirano, and H. Hosono, "Formation and decay of nonbridging oxygen hole centers in SiO_2 glasses induced by F_2 laser irradiation: In situ observation using a pump and probe technique," Appl. Phys. Lett. **79**(12), 1757 (2001).
33. K. Nagasawa, Y. Hoshi, Y. Ohki, and K. Yahagi, "Improvement of radiation resistance of pure silica core fibers by hydrogen treatment," Jpn. J. Appl. Phys. **24**(Part 1, No. 9), 1224–1228 (1985).
34. M. Tateda, N. Shibata, and S. Seikai, "Interferometric method for chromatic dispersion measurement in a single-mode optical fiber," IEEE J. Quantum Electron. **17**(3), 404–407 (1981).
35. BeamPROP by RSoft, http://www.rsoft.com
36. J. D. Love, W. M. Henry, W. J. Stewart, R. J. Black, S. Lacroix, and F. Gonthier, "Tapered single-mode fibers and devices," IEE Proc. J **138,** 343–354 (1991).
37. A. V. Yulin, D. V. Skryabin, and P. St. J. Russell, "Four-wave mixing of linear waves and solitons in fibers with higher-order dispersion," Opt. Lett. **29**(20), 2411–2413 (2004).

1. Introduction

The nonlinear generation of new wavelengths of light in fibers is of great interest as an object of study and as a technology supporting many applications. The glass-air photonic crystal fiber (PCF) greatly boosted the field because the extraordinary control provided over chromatic dispersion permits phase matching and group-velocity matching at short wavelengths down to the visible [1–4]. PCFs can also have small, tightly-confining cores, enhancing intensity for a given power. The most spectacular nonlinear interaction is supercontinuum generation, converting monochromatic light into a spectrally-broad output that is intense, coherent and in a single spatial mode, like a "white laser" beam [1,3–8]. This effort has focused on the Gaussian-like fundamental LP_{01} (or HE_{11}) mode. Its field distribution most closely resembles those of external light sources and systems like laser beams, transmission fibers or spectrometers, greatly simplifying input and output coupling.

In contrast, special mode convertors are needed to excite a single higher-order mode and return the nonlinearly-generated wave back to the LP_{01} mode at the output. In particular this second step requires broadband operation over an octave or more. Nonlinear propagation of higher modes in standard fibers has been reported over a narrow band and without conversion back to the fundamental mode [9], using grating-based mode convertors that work over tens of nanometres at most [10]. Fiber modes can be selectively excited with phase elements such as spatial light modulators [11,12] (SLMs) but these are also narrowband, with relatively high losses and the alignment and stability problems of combining bulk and fiber optics. In PCFs,

previous studies of nonlinear propagation of higher modes (as distinct from nonlinear generation of higher modes from fundamental-mode or multimode light) used an offset launch to inefficiently generate an impure higher mode and also made no attempt to produce a fundamental mode output [13–16].
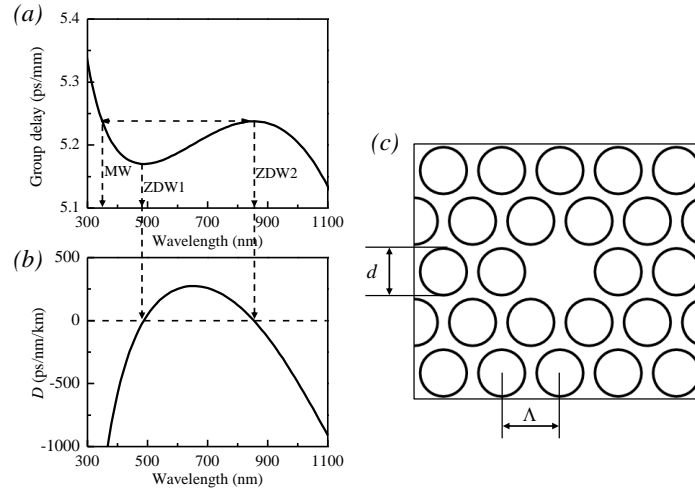

Fig. 1. Schematic group delay (a) and dispersion (b) spectra, indicating the zero dispersion wavelengths ZDW1 and ZDW2 and the matching wavelength MW. (c) Schematic PCF cross-section. We define the core diameter to be that of the largest circle that can be inscribed in the core, which for a geometrically-perfect structure is $2\Lambda - d$.

However, higher modes have desirable properties for nonlinear propagation [13,16,17]. We show that the LP_{02} (or HE_{12}) "Mexican sombrero" mode has dispersion spectra with valuable features unobtainable with the LP_{01} mode, and that light in these modes can generate much shorter wavelengths, in principle down to 240 nm in contrast with 305 nm for LP_{01}. To show how this can be realized we made low loss (< 0.5 dB) broadband (< 400 nm to >1200 nm) mode convertors by post-processing a PCF [18]. Size changes along specified air holes cause input LP_{01} waves to evolve into output LP_{02} waves and vice versa. Unlike those in [18], the new mode convertors couple the LP_{02} mode into the original unprocessed fiber core, permitting nonlinear interactions along an indefinite fiber length. The structure's adiabaticity, and the lack of any resonant basis to its operation, make it efficient and low-loss across all the fiber's guided wavelengths. In this way we generated a supercontinuum in the LP_{02} mode, and coupled it back into the more-useful LP_{01} mode over the full octave bandwidth of the supercontinuum.

2. Simulation of dispersion properties

Supercontinuum generation depends on dispersion [6–8,19–21]. Schematic spectra of group delay and group velocity dispersion D are plotted in Fig. 1(a)–1(b). The dispersion has two zeros (and the group delay two local extrema) at the zero-dispersion wavelengths ZDW1 and ZDW2. The matching wavelength MW is the wavelength shorter than ZDW1 at which the group delay matches that at ZDW2 [20].

Supercontinuum is broadest for pump light with a wavelength slightly longer than ZDW1 [3,6,7,19], where dispersion is anomalous ($D > 0$). In the regime of long pump pulses, the solitons that are created trap dispersive waves that are group-delay matched to the soliton but at a wavelength shorter than ZDW1. As each soliton self-frequency shifts to longer wavelengths, the dispersive wave shifts to shorter wavelengths to maintain the group delay match [19] until the soliton can no longer propagate. Given enough power and distance, this usually happens as the soliton reaches ZDW2, beyond which dispersion is normal ($D < 0$) and solitons cannot exist. MW as defined above is then the shortest possible supercontinuum

wavelength. However, the soliton dissipates sooner if it reaches any high-loss wavelength λ_{loss} between ZDW1 and ZDW2, in which case MW matches the group delay at λ_{loss} rather than ZDW2 [8,20]. We will take λ_{loss} = 2500 nm for dry silica [20], though hydroxyl in the glass can create such an attenuation barrier at $\lambda_{loss} \approx 1400$ nm. On averaging many different pulses with solitons shifting to different extents [6,7], the spectrum between MW and ZDW2 (or λ_{loss}) is filled with light - a supercontinuum. The wavelengths MW and ZDW2, deduced from the group delay plot, therefore delimit the attainable supercontinuum [20].
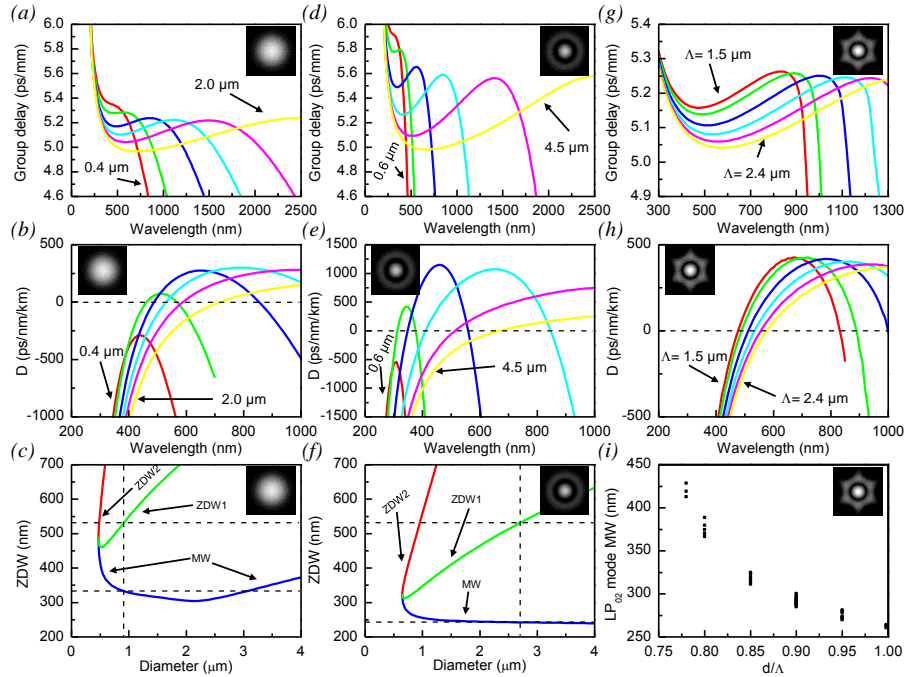

Fig. 2. Calculated group delay (a) and dispersion (b) spectra for the LP_{01} mode of a microwire, for (left to right) diameters of 0.4, 0.5, 0.7, 0.9, 1.2 and 2.0 µm. (c) Variations of key LP_{01} mode dispersion wavelengths with microwire diameter. The diameter corresponding to ZDW1 = 532 nm, and the corresponding MW, are indicated. (d-f) As (a-c) but for the LP_{02} mode and respective diameters 0.6, 0.7, 1.0, 1.5, 2.5 and 4.5 µm. (g,h) As (a,b) but for the LP_{02} mode of a PCF with d/Λ = 0.85 and (left to right) Λ = 1.5, 1.6, 1.8, 2.0, 2.2 and 2.4 µm (core diameters 1.73 - 2.76 µm). (i) MW versus d/Λ for the LP_{02} mode of PCFs with various values of Λ.

To calculate dispersion, the wavelength-dependent index of silica was given by a Sellmeier fit [21]. The propagation constants β of the modes were found and numerically differentiated to yield the group delay and dispersion [21]. For a silica microwire - a thread of silica glass surrounded by air [22,23] - β was found by solving the eigenvalue equation [24]. For PCFs, it was found by a vector plane-wave simulation [25].

The microwire is a convenient approximation for extreme PCFs with large air holes d/Λ [26], yielding a lower bound on MW. Figure 2(a)–2(b) are group delay and dispersion spectra for the fundamental LP_{01} mode, and Fig. 2(c) is a plot of ZDW1, ZDW2 and MW versus microwire diameter. (The kink in the MW curve at 2.1 µm diameter is where ZDW2 = 2500 nm and soliton propagation becomes bounded by loss.) The minimum ZDW1 and MW are 460 nm and 304 nm respectively, and a diameter near 0.9 µm matches ZDW1 to the 532 nm output of a frequency-doubled Nd:YAG laser. Such small cores complicate input coupling and are susceptible to damage and nonlinear losses, limiting the supercontinuum power [23,27].

The calculations are repeated in Fig. 2(d)–2(f) for the "sombrero" LP_{02} mode. The features are broadly similar but with greater overall dispersion [16,17,28], and particular ZDW1 and

MW values occurring at bigger diameters. For example, a diameter of 2.7 μm gives ZDW1 = 532 nm. More significantly, ZDW1 and MW themselves are much shorter. The case where ZDW1 = 532 nm gives MW = 243 nm (instead of 333 nm for LP_{01}), and the minimum ZDW1 and MW are now 312 nm and 238 nm respectively. The shortest supercontinuum wavelength is therefore over 60 nm shorter for LP_{02} than for LP_{01}, and the shortest wavelength for a 532 nm pump is 90 nm shorter. These are large differences for ultraviolet light.

The group delay, dispersion and MW for the LP_{02} mode of some PCFs are plotted in Figs. 2(g)–2(i), confirming the microwire as a good limiting model for PCFs with large d/Λ.
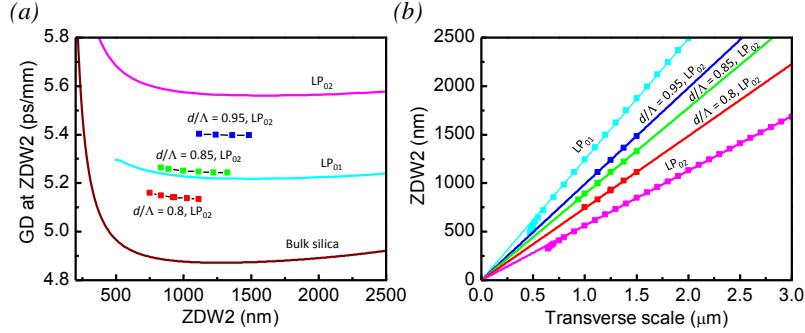

Fig. 3. (a) Group delay GD at ZDW2 versus ZDW2 (as varied by changing the scale of the fiber), for the LP_{01} and LP_{02} modes of a microwire (curves) and the LP_{02} modes of three PCFs (points). GD in bulk silica is also plotted. (b) ZDW2 versus scale for the same fibers (points), with fits to straight lines through the origin. The transverse length scale is the diameter for microwires and $\Lambda/1.6$ for PCFs: the arbitrary factor of 1.6 is chosen simply to avoid overlapping the microwire data. All results include material dispersion.

We see in Figs. 2(a), 2(d), 2(g) and Fig. 3(a) that the peak group delay (at ZDW2) for a given mode and type of fiber (microwire, or PCF of given d/Λ) is insensitive to ZDW2, even though ZDW2 itself varies strongly with scale (microwire diameter, or PCF pitch Λ). Suppose a fiber with a structure characterized by transverse length scale L has a mode whose propagation constant and group delay vary with frequency ω_0 as $\beta_0(\omega_0)$ and $\beta_{1,0}(\omega_0)$ respectively. By length-scale invariance [29], in the absence of material dispersion a fiber with the same structure but of transverse scale αL (ie, dilated by α) must support the same mode with propagation constant $\beta(\omega) = \beta_0(\omega_0)/\alpha$ at frequency $\omega = \omega_0/\alpha$, since the refractive indices are constant. The group delay is now

$$\beta_1(\omega) = \frac{d\beta}{d\omega} = \frac{1}{\alpha}\frac{d\beta_0}{d\omega_0}\frac{d\omega_0}{d\omega} = \beta_{1,0}(\omega_0) = \beta_{1,0}(\alpha\omega). \qquad (1)$$

The group delay curve for the scaled fiber is therefore the same as for the unscaled fiber but compressed by α along the ω axis (or, stretched by α along a wavelength axis). Thus in the absence of material dispersion the peak group delay is constant for a given mode in a given fiber structure, and ZDW2 is proportional to the scale.

This is approximately true even with material dispersion because, for wavelengths longer than 500 nm, the group delay of bulk silica (Fig. 3(a)) varies little compared to its difference from that of the modes. However, the material group delay rises rapidly for shorter wavelengths and dominates the group delay of the modes too, Fig. 2(a), 2(d) and 2(g). Thus the group delay at ZDW2 is matched at similar short wavelengths MW regardless of the fiber's scale, giving very flat LP_{02} MW curves, Fig. 2(f) and 2(i). In Fig. 2(i) the group delay at ZDW2 (and hence MW) is changed by the relative hole diameter d/Λ, but not by the scale Λ. A wide range of pump sources (with different ZDW1 requirements) should therefore give similar minimum supercontinuum wavelengths for this mode. In contrast the MW curve is not so flat for the LP_{01} mode, and the minimum supercontinuum wavelength is only available for

particular pump wavelengths or by using non-uniform fibers to vary dispersion with distance [4,8]).

3. PCF fabrication

Two silica-air PCFs were designed to have an LP_{02} mode ZDW1 slightly shorter than the pump wavelength of 532 nm. The hole diameter d, pitch Λ and inscribed-circle core diameter were respectively 1.86, 2.09 and 2.25 μm for fiber 1, Fig. 4(a), and 1.86, 2.05 and 2.13 μm for fiber 2. (The core diameters were smaller than $2\Lambda - d$ because the innermost six holes were slightly elongated towards the core.)
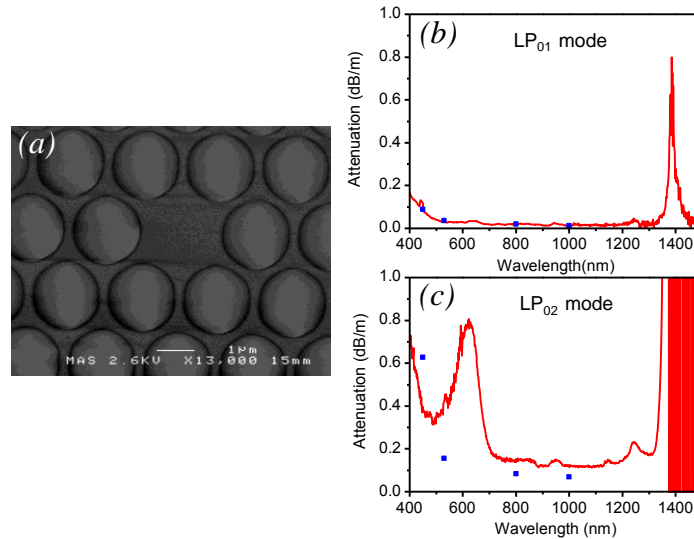

Fig. 4. (a) SEM of fiber 1. (b,c) Measured attenuation spectra for fiber 1's LP_{01} (b) and LP_{02} (c) modes. The points are more-reliable single-wavelength measurements.

We measured the attenuation of fiber 1 for the LP_{01} and LP_{02} modes by the cut-back technique, from the ratio of transmission measurements with different lengths of fiber, Fig. 4(b)–4(c). We used a mode filter and mode convertor to select just the LP_{01} mode and just the LP_{02} mode respectively. The mode filter and mode convertor, and the measurement equipment, are described in Section 5. The minimum attenuation at 1000 nm was 0.07 dB/m for LP_{02} and < 0.02 dB/m for LP_{01}.

Figure 4(b)–4(c) exhibit known features of the attenuation spectra of silica fibers. For LP_{01}, Fig. 4(b) shows rising UV attenuation from Rayleigh scattering in silica and surface scattering around the small PCF core. Standard Ge-doped fibers have a strong absorption edge at 380 nm: its absence in the undoped PCF allows the short-wavelength transmission shown later in Figs. 9(c)–9(e). The fiber was made without drying or annealing and so absorbs strongly at 1380 nm due to OH [30]. For LP_{02}, Fig. 4(c) has a similar but stronger UV edge due to the mode's greater overlap with the core boundary, causing more surface scattering. The steep edge at 1350 nm is due to LP_{02} mode cutoff rather than OH absorption.

The 630 nm feature in Fig. 4(c) seems to be a non-bridging oxygen hole center (NBOHC) absorption [31], known as a drawing band because NBOHCs can be created during fiber drawing [30]. In this case it is not caused by drawing as it is absent in the LP_{01} measurement of as-drawn fiber. However, the fiber of Fig. 4(c) had already been used for supercontinuum experiments and subjected to intense UV pulses, a known cause of NBOHCs and hence photodarkening at 630 nm [32]. Hydrogen or deuterium loading [33] can reduce it by terminating the NBOHCs (as -OH or -OD). The consequent infrared absorption does not overlap with wavelengths of interest here.

LP_{01} dispersion spectra were measured by white-light interferometry [34], giving ZDW1 values of 789 and 777 nm for fibers 1 and 2 respectively, Fig. 5(a)–5(b). It is not simple to measure dispersion spectra of higher-order modes [17] so we calculated them from scanning electron micrographs (SEMs) of the fibers, Fig. 5(b). The calculated LP_{01} mode ZDW1 matched the measurements to within a nanometer, and the calculated LP_{02} mode ZDW1 values were 527 and 515 nm respectively.

Although SEMs suffer from uncertainties in calibration and locating hole boundaries, the inference of LP_{02} ZDW1 from a known LP_{01} ZDW1 is actually insensitive to the structure. To demonstrate this, the relationship between ZDW1 for the two modes was simulated for PCFs with d/Λ of 0.78-1.00 and Λ of 1.5-2.6 μm, Fig. 5(c). We include structures where the innermost holes were given oval distortions to simulate deformation during fiber fabrication, reducing the core diameter by up to 20% compared to an undeformed structure. (The same data set was used for Fig. 2(i).) There is a very close correlation between LP_{01} and LP_{02} ZDW1 values, even for widely different PCFs. We therefore have confidence in the simulated values for LP_{02} ZDW1 despite any SEM inaccuracies: using Fig. 5(c) the measured LP_{01} ZDW1 determines LP_{02} ZDW1 to within ± 5 nm anyway.
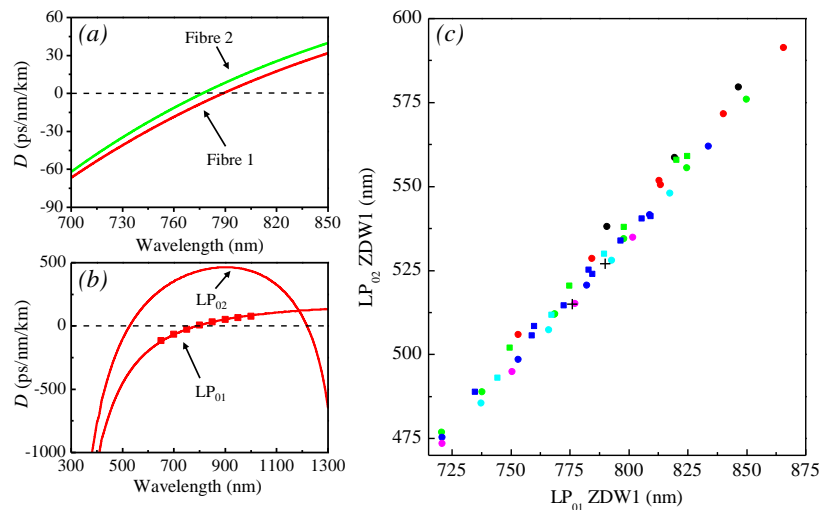

Fig. 5. (a) Measured LP_{01} dispersion spectra for both fibers. (b) Simulated LP_{01} and LP_{02} dispersion spectra for fiber 1. The points are measured LP_{01} values from (a). (c) Calculated relation between LP_{02} ZDW1 and LP_{01} ZDW1 for PCFs with differing Λ, d/Λ and distortions of the innermost holes. Round points are undistorted, square points have distortions, d/Λ = 0.78 (black), 0.80 (red), 0.85 (green), 0.90 (blue), 0.95 (cyan), 0.998 (magenta). The crosses are simulations of experimental fibers 1 and 2.

4. Simulation of the mode convertor

Figure 6(b) shows cross-sectional optical micrographs along a typical mode convertor in fiber 1, cleaved at locations A-H. The structural changes were gradual except for the sudden appearance of a parasitic annular core between A and B over a distance of < 2 mm. In our later experiments, a second mode convertor with the same transition but in reverse order (H′-A′) coupled the LP_{02} mode back into the LP_{01} mode. Note that the input and output structures at A and H were the original untreated fiber, which can be arbitrarily long.

The fields at locations A-H for an LP_{01} mode input, Fig. 6(a), were simulated by the scalar beam propagation method [35] (BPM) for a fiber with the same hole size and pitch as fiber 1 and a wavelength of 532 nm. Holes changed size linearly without lattice deformation in the model transitions. The section lengths were 0 mm (A-B), 10 mm (B-D), 10 mm (D-F) and 10 mm (F-H). The second identical but reversed mode convertor H′-A′ followed 10 mm of

uniform fiber, with 10 mm of uniform fiber beyond H′ to allow unguided light to diffract away. Loss and mode purity could be calculated from overlap integrals of the output with the appropriate modes, all found using the same software.
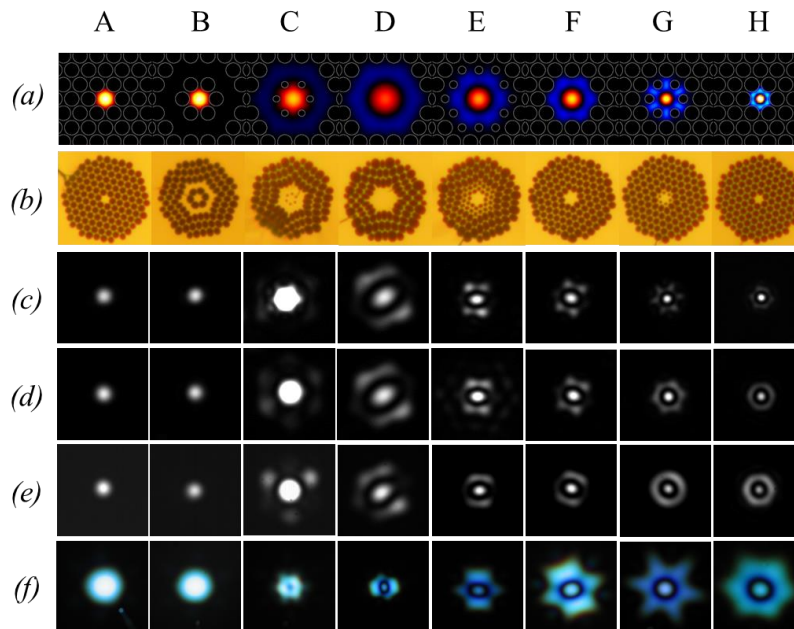

Fig. 6. Cross sections at locations A-H along a forward mode convertor. (a) Simulated fields for an LP$_{01}$ input at A (Media 1, includes a reverse mode convertor H′-A′ beyond H). Red/blue indicate opposite phases, grey circles are hole boundaries. (b) Optical micrographs of an experimental structure made from fiber 1, to the same scale. The holey region at locations A and H is 23 μm across. (c-e) Measured near-field patterns for light with wavelengths of (c) 400 nm, (d) 800 nm and (e) 1100 nm. (f) Measured far-field patterns for white light.

The structure is adiabatic (light stays in a given order of mode of given symmetry) except between A and B, where the abruptly-appearing annular core changes the mode order. The fundamental mode of the composite two-core waveguide at B now occupies the (larger) annular core, the original light finding itself in a higher mode of the same symmetry. This is therefore where mode conversion occurs. However, only the label "fundamental mode" moves to the annular core: the light stays in the central core and its field distribution is unaffected. Calculations confirm that the fundamental mode at B (the mode with the greatest propagation constant β) fills the annular core with uniform phase, Fig. 7(a). The mode in the central core, Fig. 7(b), is in fact the spatial mode of 10th greatest β. The intervening 8 modes occupy the annular core with phase variations, one being plotted in Fig. 7(c) - they do not have the same symmetry as the input wave, and so play no role in symmetric mode convertors.

The non-adiabatic transition A-B does not need to be abrupt on a practical scale, just much shorter than the directional-coupling length where the cores are phase-matched [36]. We estimate this to be of the order of a meter for 532 nm light, so the "abrupt" transition can be quite long in practice. A simulation of a 10 mm transition between A and B showed that the loss of light from the central core was < 0.0001 dB at this wavelength.
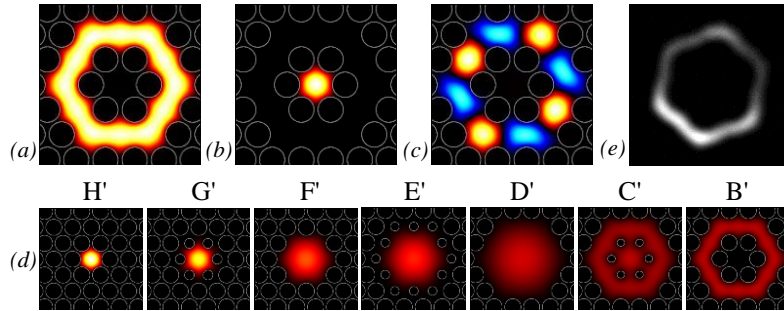
Fig. 7. (a)–(c) Calculated fields at B, for (a) the fundamental mode, (b) the 10th mode and (c) the 9th mode. (d) Simulated fields at locations H′-B′ along a reverse mode convertor, for an LP$_{01}$ input at H′ (Media 2). An LP$_{02}$ input at H′ would give the reverse of Fig. 6(a). (e) Experimental near-field pattern at the end of a reverse transition H′-B′, for input light of wavelength 800 nm in the LP$_{01}$ mode at H′.

Beyond B the first ring of holes gradually shrink and disappear to form one big core at D. Light remains in the higher mode, now recognizably an LP$_{02}$ "sombrero", after this adiabatic transition. Our previous LP$_{02}$ mode convertor ended here [18] but the core at D is too big, too poorly-controlled and too limited in length (a few centimeters) to be a good nonlinear medium. Therefore in the new section D-H the vanished holes reappear gradually: first the second ring (D-F) then the first ring (F-H). This shrinks the core and adiabatically squeezes the LP$_{02}$ mode into the core of the original unprocessed fiber. The mode can now propagate in this small, well-controlled core along a distance limited only by the fiber length.

The simulated transmission loss for 532 nm input light in the LP$_{01}$ mode was 0.0015 dB to the LP$_{02}$ mode after the first (forward) mode convertor of Fig. 6(a), and 0.0025 dB to the LP$_{01}$ mode after the second (reverse) mode convertor. For 1000 nm light the respective losses were 0.003 dB and 0.005 dB, illustrating efficiency and a broad wavelength range. For both wavelengths and locations the mode purity was better than 34 dB.

Light in the annular mode at B should evolve adiabatically into the central LP$_{01}$ mode at H and vice versa. We simulated the evolution of LP$_{01}$ light at H′ through a reverse mode convertor to B′ - see Fig. 7(d) and Media 2, in contrast to Fig. 6(a) (from right to left) and the second half of Media 1. The output was indeed in the annular mode, with 0.05 dB loss.

5. Fabrication and characterization of mode convertors

Figure 8 shows our experimental setup. We made mode convertors by heating a fiber with a small flame, applying pressure to holes being kept open but not to holes being collapsed. Hole size transitions were formed by varying the motion of the flame [18], Fig. 6(b). Furthermore, to provide a pure LP$_{01}$ mode at the input even though the fiber was multimode, we heated ~6 cm of fiber at the input to shrink all the holes by ~70%, Fig. 8(a). This makes the fiber locally single-mode and acts as a mode filter. Each sequence (mode filter, one or two mode convertors, and lengths of fiber before, after or between them) for a particular experiment was made on a continuous fiber: there were no splices, or cleaves except at beginning and end. Typical section lengths were 1-2 mm (A-B), 10 mm (uniform B), 10 mm (B-D), 20 mm (uniform D), 20 mm (D-F), 15 mm (uniform F) and 20 mm (F-H).

For simplicity our simulations assumed that holes close and open without deforming the lattice, creating glass to preserve unit cell area as a hole shrinks. In reality glass is conserved, leaving a much thinner annular core in experiments than in simulations. To make a wide-enough annular core at B we therefore collapsed the third ring of holes as well as the second. This is most visible at E in Fig. 6(b). It was necessary here but not in [18] because d/Λ is much greater here, leaving less glass in the unit cell when a holes closes.
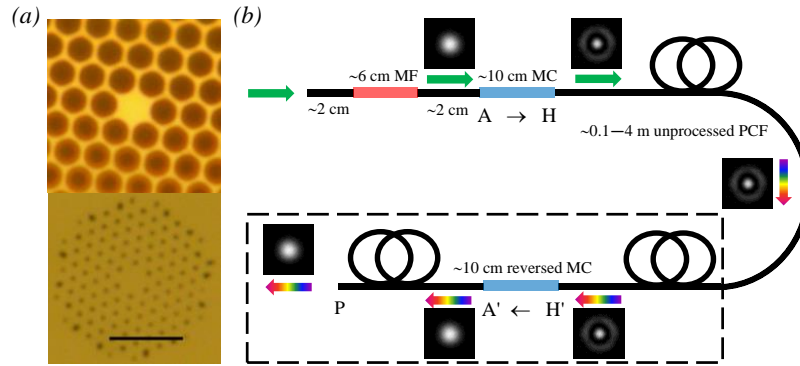
Fig. 8. (a) Optical micrographs (to the same scale, 5 μm scale bar) of fiber 1 before (top) and after (bottom) heating to form a mode filter. (b) Setup with mode filter (MF) at the input of a mode convertor (MC) followed by untreated fiber. The dotted box shows the reversed MC and further fiber used in the final experiments.

Light patterns (Figs. 6, 7 and 11) were measured using an LP_{01} supercontinuum [8] coupled into the fiber under test. (This standard laboratory white-light source is distinct from the LP_{02} mode supercontinuum that is our object of study.) Unfiltered far-field patterns projected onto paper were recorded using a consumer digital camera. Near-field patterns were imaged onto a lens-less camera using a $40 \times$ microscope objective (NA = 0.65) via 10 nm bandpass filters. The camera was a CCD for 400-1000 nm light and an InGaAs array for 1100 nm and beyond. The near-field images in Fig. 6(e) are therefore not to the same scale as those in Fig. 6(c)–6(d), and similarly for short and long wavelengths in Fig. 11.

After imaging the mode convertor output when cleaved at location H, it was cut back to inspect intermediate locations, Fig. 6(c)–6(f). (The images for C were over-exposed to highlight faint peripheral features - no such features were visible in similarly over-exposed images at B, not shown.) The measured patterns compare well qualitatively with the simulated patterns and with each other, and confirm that the input at A was indeed in the LP_{01} mode. The patterns in the enlarged core at D were less symmetric than in the simulation, probably because the post-processed core was imperfectly symmetric. However, the outputs at H are clear LP_{02} modes across the whole wavelength range from 400 to 1100 nm. Examination of the dark ring in the near-field images indicates an LP_{02} mode purity of at least 20 dB [18].

We tested the behavior simulated in Fig. 7(d) by launching LP_{01} light into location H′ of a reversed mode convertor via a mode filter. The output at cleaved location B′ was in an annular mode, Fig. 7(e), as expected.

We measured loss spectra by the cut-back technique before and after removal of the device under test, using a laser-driven xenon discharge source (Energetiq, EQ99) and an optical spectrum analyzer (OSA, Ando AQ6315B). However, absolute loss values were unreliable because the more-divergent LP_{02} mode was less well-coupled into the OSA than the LP_{01} mode, so accurate single-wavelength measurements were also made using bandpass-filtered light and a large-area photodiode to collect all of the LP_{02} light. The loss of a typical mode convertor was < 0.5 dB across the 450-800 nm wavelength range, and as low as 0.1 dB at some wavelengths.

6. Supercontinuum generation in the LP_{02} mode

The pump source was a 532 nm frequency-doubled Nd:YAG microchip laser emitting 0.6 ns pulses with a repetition rate of 7.0 kHz and an average power of 24 mW. These effectively-CW pulses were long compared to any dispersion imposed by the lengths of fiber in our experiments. The laser light was coupled into the mode convertors (via a mode filter) with ~30% efficiency. Output spectra were measured using the OSA - the step at 600 nm is a

calibration artifact at a change of order-sorting filter. However, the short-wavelength spectrum for fiber 2 was determined using a UV spectrometer (Bentham DTMc300).

Output spectra for LP_{02} mode propagation along 1.8 m of each fiber beyond location H show modulation instability [21] (MI) at low power and a supercontinuum at higher power, Fig. 9. The MI sidebands indicate anomalous dispersion at 532 nm, as expected from the simulated LP_{02} ZDW1 of 527 nm for fiber 1. The LP_{02} ZDW1 of 515 nm for fiber 2 is even shorter so we see closer MI sidebands. Given the MI wavelengths, measured output powers (assuming gaussian pulses and zero loss) and calculated LP_{02} effective areas, from chapter 5 of [21] we estimate the dispersion at 532 nm to be around 30 and 125 ps nm^{-1} km^{-1} in fibers 1 and 2 respectively. The simulated values of 15 and 60 ps nm^{-1} km^{-1} have a similar ratio but different absolute values, probably due to common factors like conversion from average power to peak intensity. The simulated dispersion spectrum of fiber 2 predicts a phase-matched dispersive wave [37] at 483 nm, evident in Fig. 9(b) and 9(e). In both fibers the spectra extend below 375 nm for our maximum available power, and for fiber 2 extends to 330 nm, Fig. 9(d). The output powers were higher and the devices considerably more durable than when using the same 532 nm laser for the LP_{01} mode, which required submicron core diameters [23]. The output spectra were also broader, even though the larger core diameter means that the peak intensity is reduced. Here the output pattern was a clear LP_{02} mode in all cases, bottom row insets of Fig. 11(b).
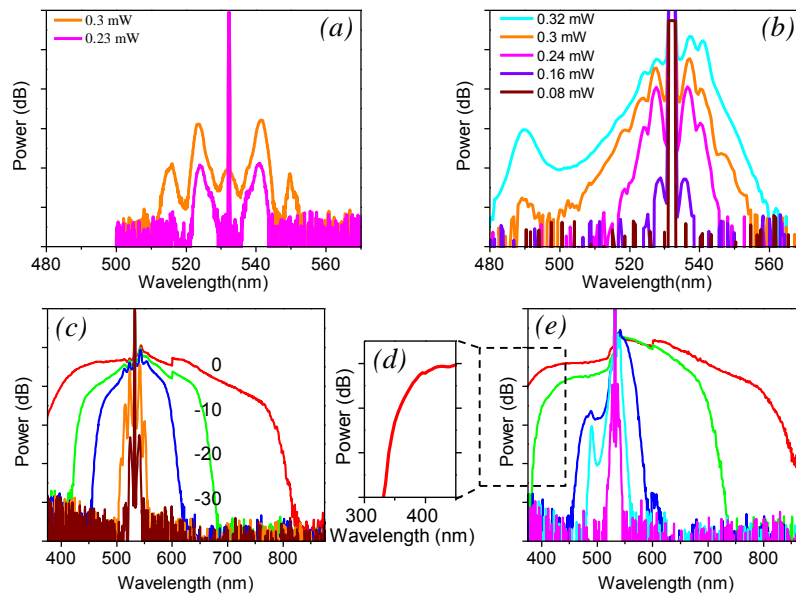

Fig. 9. (a,b) Low power LP_{02} output spectra for 1.8 m of fibers 1 and 2 respectively, with MI sidebands in both fibers and a dispersive wave at 490 nm for fiber 2. (c,e) As (a,b) for higher output powers leading to supercontinuum (outer to inner traces) of (c) 1.9, 1.1, 0.60, 0.30, and 0.19 mW and (e) fiber 2 at 1.9, 1.2, 0.49, 0.32, and 0.24 mW. (d) The UV end of spectrum (e) for 1.9 mW. Vertical scales 10 dB per division, resolutions (a) 0.2 nm, (b,c,e) 2 nm, (d) 5 nm.

Shortening the fibers beyond location H yielded a reduced bandwidth, Fig. 10(a)–10(c). With just 10 cm of fiber 1 beyond H we observed no broadening at all except at an output power exceeding 3 mW, when we saw weak MI sidebands resembling those in Fig. 9(a). This confirmed that broadening was insignificant before the LP_{02} mode was generated.

The shortest supercontinuum wavelength we observed in all our experiments was 320 nm, a little shorter than the minimum in Fig. 9(d). This is longer than the ~250 nm minimum predicted in Fig. 2(f) and 2(i) because of the limited available pump power. Linear attenuation or two-photon absorption at the short-wavelength edge would limit the spread of dispersive waves into the UV, but would not stop the associated solitons from shifting further into the

infrared. The long- and short-wavelength edges of the supercontinuum were group-delay matched as expected [19,20]. Figure 10(d) and 10(e) show the calculated group delay at the edges of all spectra in Figs. 9 and 10 with high-enough power to establish soliton self-frequency shifting and a well-determined short-wavelength edge. Different choices of the (arbitrary) power level defining the edges made no qualitative difference. Although the lines joining the edge wavelengths are not quite horizontal, the group-delay curve is so steep at short wavelengths that small wavelength changes are enough to match the group delays exactly.
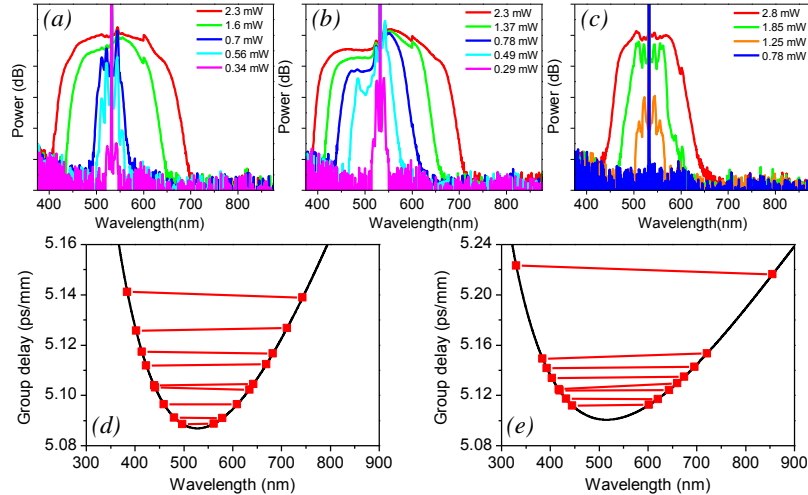

Fig. 10. (a,b) LP_{02} output spectra for 0.8 m of fibers 1 and 2 respectively. (c) Corresponding spectrum for 0.3 m of fiber 1. Vertical scales 10 dB per division, resolution 2 nm. (d,e) Calculated group delay (black) for (d) fiber 1 and (e) fiber 2, with measured pairs of supercontinuum edge wavelengths (red) for a range of fiber lengths and output powers.

This close match of group delay suggests that power and/or fiber length are limiting the UV extent of the continuum in these LP_{02} experiments. The UV spectrum may therefore be improved with a different pump source. In contrast, for LP_{01} supercontinuum pumped by the equivalent 1064 nm laser the short wavelength extent is limited by group delay matching [20] and so can only reach <350 nm using non-uniform fibers [4,8]. Indeed it is possible that the UV spectrum with the LP_{02} mode can be shortened even more using non-uniform fibers.

7. Conversion to fundamental-mode output

To couple light back into the LP_{01} mode and provide an output compatible with other optical systems, a practical higher-mode device needs another mode convertor [28], which for supercontinuum generation must be broadband across more than an octave. We therefore made a second, reversed, mode convertor at the end of the previous structure (H′ to A′ in Fig. 8(b), dashed box), with 4 m of fiber 1 between the mode convertors and 0.9 m of fiber beyond the second one ending at location P. Figure 11(a) shows light patterns at the output P, and at H′ (after removing the second mode convertor), for broadband input light. As intended, the LP_{02} mode at H′ became an LP_{01} mode at P.

Supercontinuum spectra generated in the LP_{02} mode (measured at H′) but output in the LP_{01} mode (measured at P) are plotted in Fig. 11(b). The whole spectrum was efficiently converted to the fundamental mode, but broadened further in the final 0.9 m between A′ and P. Nonlinear processes continued for the high-intensity broadband light in the LP_{01} mode: the measured LP_{01} ZDW1 was 789 nm so intense light at this wavelength can generate further supercontinuum. In Fig. 11(b) there is a spectral notch near 800 nm, indicating light converted from the LP_{01} ZDW1 to longer and shorter wavelengths.
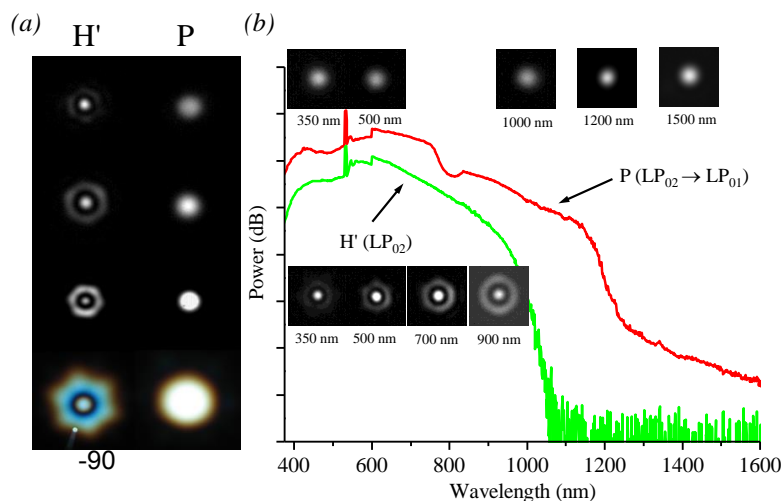
Fig. 11. (a) Light patterns at (left) the input H′ and (right) the output P of a second, reversed, mode convertor, after linear propagation of white light. Top to bottom; near field at 400, 800 and 1100 nm, and far field for white light. (b) Output supercontinuum spectra and near-field patterns generated in 4 m of fiber between the two mode convertors, before (P) and after (H') the second one was removed. The vertical offset of the traces is due to arbitrarily-different coupling into the OSA: the total output powers were 1.60 mW (H') and 1.55 mW (P). Vertical scale 10 dB per division, resolution 5 nm.

8. Discussion and conclusions

We have extended nonlinear fiber optics to higher modes using all-fiber mode convertors that are non-resonant, broadband and low-loss, leading to LP_{02} supercontinuum generation in PCFs where both input and output can be in the fundamental mode. The dispersion and nonlinear properties of the LP_{02} mode are broadly similar to those of the fundamental mode, but the key dispersion wavelengths are much shorter and occur for larger cores. The mode can therefore generate shorter-wavelength UV light from shorter-wavelength pump sources in fibers that are more damage-resistant and easier to couple into.

This is important for applications requiring visible or ultraviolet continuum, such as fluorescence microscopy. Most systems, stains and markers are designed for visible light, and many biological structures exhibit signature autofluorescence from UV excitation. Although efficient and rugged 532 nm lasers are available, current visible supercontinuum sources use pump lasers emitting the much-longer wavelengths of 800 or 1064 nm [7] because fibers with the appropriate LP_{01} dispersion at 532 nm have submicron-diameter cores [23]. Sub-micron core diameters present input coupling difficulties and are susceptible to damage and nonlinear losses at modest input power, limiting the supercontinuum power. In contrast, zero-dispersion wavelengths as short as 310 nm are possible with the LP_{02} mode (compared to 460 nm for LP_{01}), giving a predicted short-wavelength supercontinuum edge down to 240 nm (compared to 305 nm for LP_{01}). These desirable properties can be achieved for core diameters as big as 2.6 μm. We have demonstrated supercontinuum generation pumped by sub-nanosecond pulses at 532 nm in fibers with > 2 μm core diameter and generated wavelengths as short as 330 nm for estimated peak powers of < 600 W.

This is just one example of how higher modes provide new dispersion properties to be exploited for nonlinear interactions. Other examples include the combination of higher-mode and fundamental-mode interactions at different places along a fiber, Fig. 11(b), and the generation of discrete short wavelengths by four-wave mixing in fibers with normal dispersion [2,3]. These can of course be generalized to other modes besides LP_{02}. Our mode convertors provide a low-loss and broadband tool for realizing this unexplored space of possibilities.

Acknowledgments